

Tripartite Quantum State Sharing

Andrew M. Lance,¹ Thomas Symul,¹ Warwick P. Bowen,¹ Barry C. Sanders,² and Ping Koy Lam¹

¹Quantum Optics Group, Department of Physics, Faculty of Science, Australian National University, ACT 0200, Australia

²Quantum Information Science Group, Department of Physics and Astronomy, University of Calgary, Alberta T2N 1N4, Canada

(Dated: October 26, 2018)

We demonstrate a multipartite protocol to securely distribute and reconstruct a quantum state. A secret quantum state is encoded into a tripartite entangled state and distributed to three players. By collaborating, any two of the three players can reconstruct the state, whilst individual players obtain nothing. We characterize this (2, 3) threshold quantum state sharing scheme in terms of fidelity, signal transfer and reconstruction noise. We demonstrate a fidelity averaged over all reconstruction permutations of 0.73 ± 0.04 , a level achievable only using quantum resources.

Secret sharing[1] is a powerful technique in computer science, which enables secure and robust communication in information networks, such as the internet, telecommunication systems and distributed computers. The security of these networks can be enhanced using quantum resources to protect the information. Such schemes have been termed *quantum secret sharing*[2]. Many applications in quantum information science, however, require the distribution of quantum states. One such example are quantum information networks, which are expected to consist of nodes where quantum states are created, processed and stored, connected by quantum channels[3]. It is of paramount importance that the quantum channels in these networks allow the robust and secure distribution of quantum states between nodes. Cleve *et al.*[4] proposed the secret sharing of quantum states as a protocol that provides these capabilities, overcoming failures or conspiracies by nodes. We term this *quantum state sharing* to differentiate from the quantum secret sharing of classical information. In (k, n) threshold quantum state sharing[4], the “dealer” node encodes a secret state into an n -party entangled state and distributes it to n “player” nodes. Any k players (the access structure) can collaborate to retrieve the quantum state, whereas the remaining $n - k$ players (the adversary structure), even when conspiring, acquire nothing. This scheme provides quantum information networks with a secure framework for distributed quantum computation and quantum communication.

The original quantum state sharing scheme by Cleve *et al.* was formulated for discrete states and requires the control and coupling of qudits (d -dimensional extensions of qubits), which is extremely experimentally challenging. In the continuous variable regime, however, quantum state sharing is feasible utilizing Einstein-Podolsky-Rosen (EPR) entanglement[5], an experimentally accessible quantum resource[6, 7]. We demonstrate (2, 3) threshold quantum state sharing in this regime. In our scheme, a secret coherent state is encoded into a tripartite entangled state and distributed to three players. We demonstrate that any two of the three players can form an access structure to reconstruct the state. The state reconstruction is characterized in terms of fidelity, signal transfer, and reconstruction noise. These measures show a direct verification of our tripartite continuous variable entanglement. As coherent states form an over-

complete basis for all quantum states, arbitrary states can be shared by this scheme.

The quantum states of interest in this paper reside at the frequency sidebands of an electromagnetic field. In the Heisenberg picture of quantum mechanics, a quantum state can be represented by the field annihilation operator $\hat{a} = (\hat{X}^+ + i\hat{X}^-)/2$, where $\hat{X}^\pm = \langle \hat{X}^\pm \rangle + \delta \hat{X}^\pm$ are the amplitude (+) and phase (-) quadratures, with variances of $V^\pm = \langle (\hat{X}^\pm)^2 \rangle$. In our dealer protocol, the dealer interferes the secret state \hat{a}_{in} with one of a pair of EPR entangled beams \hat{a}_{EPR1} on a 1:1 beam splitter (Fig. 1). The two output fields and the second entangled beam \hat{a}_{EPR2} form the three shares which are distributed to the players. The entangled state ensures that the secret is protected from each player individually and is generated by interfering a pair of amplitude squeezed beams \hat{a}_{sqz1} and \hat{a}_{sqz2} [7]. The dealer can further enhance the security of the scheme by displacing the coherent amplitudes of the shares with correlated Gaussian white noise[8]. Choosing the Gaussian noise to have the same correlations as the quadrature entanglement, the shares can be expressed as

$$\hat{a}_1 = (\hat{a}_{\text{in}} + \hat{a}_{\text{EPR1}} + \delta\mathcal{N})/\sqrt{2} \quad (1)$$

$$\hat{a}_2 = (\hat{a}_{\text{in}} - \hat{a}_{\text{EPR1}} - \delta\mathcal{N})/\sqrt{2} \quad (2)$$

$$\hat{a}_3 = \hat{a}_{\text{EPR2}} + \delta\mathcal{N}^* \quad (3)$$

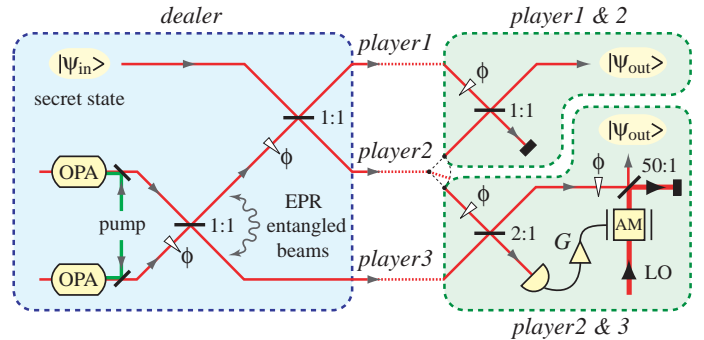


FIG. 1: Schematic of the (2, 3) quantum state sharing scheme. ψ_{in} : secret quantum state, OPA: optical parametric amplifier, G : electronic gain, AM: amplitude modulator, LO: optical local oscillator. $x:y$: beam splitter with reflectivity $x/(x+y)$ and transmittivity $y/(x+y)$.

where $\delta\mathcal{N} = (\delta N^+ + i\delta N^-)/2$ represents the Gaussian noise with mean $\langle\delta N^\pm\rangle = 0$ and variance $\langle(\delta N^\pm)^2\rangle = V_N$, and $*$ denotes the complex conjugate.

The reconstruction protocol used for the (2,3) quantum state sharing scheme is dependent on the corresponding access structure (Fig. 1). The access structure formed when players 1 and 2 collaborate, henceforth denoted $\{1,2\}$, reconstructs the secret quantum state by completing a Mach-Zehnder interferometer using a 1:1 beam splitter[5]. The access structures $\{2,3\}$ and $\{1,3\}$ reconstruct the quantum state by utilizing a 2:1 beam splitter and an electro-optic feedforward loop[8]. In the latter protocol, combining the shares on the beam splitter with appropriate relative phase reconstructs the phase quadrature of the secret state on one of the beam splitter outputs. In contrast, the amplitude quadrature has additional noise as a result of this process. This noise, however, is correlated with the amplitude quadrature of the other beam splitter output, which is detected. The resulting photocurrent is fedforward to displace the amplitude quadrature of the first output. Assuming no losses, the quadratures of the reconstructed secret can then be expressed as [8]

$$\begin{aligned}\delta\hat{X}_{\text{out}}^+ &= g^+\delta\hat{X}_{\text{in}}^+ + \frac{\sqrt{3}}{2}(1-\sqrt{3}g^+)(\delta\hat{X}_{\text{sqz1}}^+ + \delta\hat{X}_{\text{sqz2}}^+) + \\ &\quad \frac{1}{2}(g^+ - \sqrt{3})(\delta\hat{X}_{\text{sqz1}}^- - \delta\hat{X}_{\text{sqz2}}^-) + (\sqrt{3} - g^+)\delta N^+ \quad (4) \\ \delta\hat{X}_{\text{out}}^- &= \frac{1}{\sqrt{3}}(\delta\hat{X}_{\text{in}}^- + \delta\hat{X}_{\text{sqz1}}^+ - \delta\hat{X}_{\text{sqz2}}^+) \quad (5)\end{aligned}$$

where $g^\pm = \langle\hat{X}_{\text{out}}^\pm\rangle/\langle\hat{X}_{\text{in}}^\pm\rangle$ are the optical quadrature gains. The phase quadrature gain $g^- = 1/\sqrt{3}$ is set by the 2:1 beam splitter, whilst the amplitude quadrature gain $g^+ = (1/\sqrt{3} + G/\sqrt{6})$ has an additional term which is a function of the electronic feedforward gain G . We refer to the specific gain of $g^+g^- = 1$ as the *unitary gain point*. At unitary gain and in the limit of perfect squeezing, the quadratures of the reconstructed state are given by $\delta\hat{X}_{\text{out}}^\pm = (\sqrt{3})^{\pm 1}\delta\hat{X}_{\text{in}}^\pm$. This state is directly related to the secret state via a local unitary parametric operation. Although not in the same form as the secret state, such a reconstructed state is only achievable using entanglement. On the other hand, the unitary parametric operation is local and requires no entanglement. Therefore, the essence of the reconstruction protocol is contained within the feedforward scheme.

In our experiment we use a Nd:YAG laser producing a coherent field at 1064nm to provide a shared time frame between all parties; to yield the dealer secret state, produced by displacing the sideband vacuum state of the laser field using an amplitude and a phase modulator at 6.12MHz; and to produce two amplitude squeezed states generated in hemilitic MgO:LiNbO₃ optical parametric amplifiers (OPAs) pumped with 532nm light. The output fields of each OPA are squeezed 4.5 ± 0.2 dB below the quantum noise limit. These squeezed beams are interfered on a 1:1 beam splitter with an observed visibility of $99.1 \pm 0.2\%$. The beam splitter outputs are EPR entangled and satisfy the wave-function inseparability criterion $\langle(\delta\hat{X}_{\text{EPR1}}^+ + \delta\hat{X}_{\text{EPR2}}^+)^2\rangle\langle(\delta\hat{X}_{\text{EPR1}}^- - \delta\hat{X}_{\text{EPR2}}^-)^2\rangle/4 =$

$0.44 \pm 0.02 < 1$ [7, 10]. To enhance the security of the secret state against the adversaries, the coherent quadrature amplitudes of the entangled beams are displaced with Gaussian noise of variance $V_N = 3.5 \pm 0.1$ dB. Experimentally, this noise can be actively applied using electro-optic modulation techniques, but in our case it appears naturally as a result of de-coherence[16]. A homodyne detector is used to characterize the secret, adversary and reconstructed quantum states using a configuration of removable mirrors. To ensure accurate results, the total homodyne detection efficiency, $\eta_{\text{hom}} = 0.89 \pm 0.01$, is inferred out of each measurement.

We characterize the quality of the state reconstruction for the access and adversary structures using fidelity $\mathcal{F} = \langle\psi_{\text{in}}|\rho_{\text{out}}|\psi_{\text{in}}\rangle$, which measures the overlap between the secret and reconstructed quantum states[11]. Assuming that all fields involved have Gaussian statistics and that the secret is a coherent state, the fidelity can be expressed in terms of experimentally measurable parameters as

$$\mathcal{F} = 2e^{-(k^+ + k^-)/4} / \sqrt{(1 + V_{\text{out}}^+)(1 + V_{\text{out}}^-)} \quad (6)$$

where $k^\pm = \langle X_{\text{in}}^\pm \rangle^2 (1 - g^\pm)^2 / (1 + V_{\text{out}}^\pm)$. In our experiment, the fidelity for $\{1,2\}$ can be determined directly; however, for

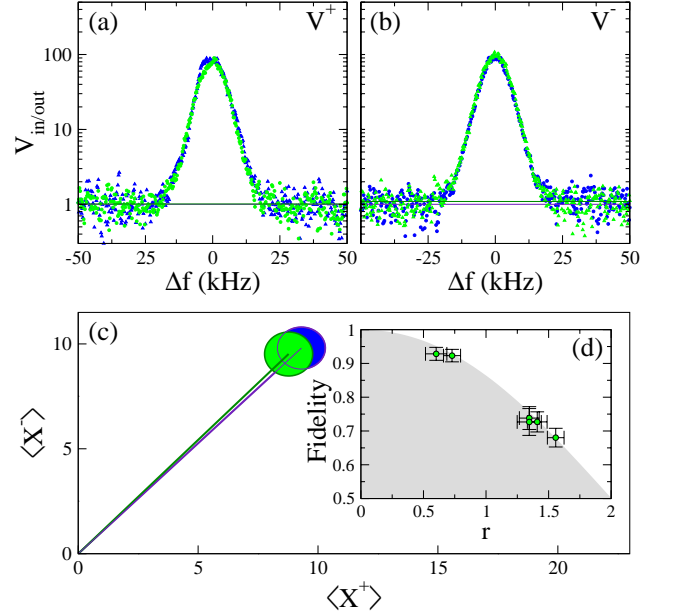


FIG. 2: Experimental results for the $\{1,2\}$ access structure. (a) and (b) show the spectra of the amplitude and phase quadrature variances for the secret (input, blue/dark grey) and reconstructed (output, green/light grey) quantum states. Δf is the offset from the signal frequency at 6.12 MHz. Resolution Bandwidth = 1 kHz, Video Bandwidth = 30 Hz. (c) Standard deviation contours of Wigner functions of the secret (blue/dark grey) and reconstructed (green/light grey) quantum states. (d) Measured fidelity as a function of gain deviation $r^2 = (\langle\hat{X}_{\text{out}}^+\rangle - \langle\hat{X}_{\text{in}}^+\rangle)^2 + (\langle\hat{X}_{\text{out}}^-\rangle - \langle\hat{X}_{\text{in}}^-\rangle)^2$. (d) Grey area highlights the accessible fidelity region. Points plotted are from six different experimental runs.

$\{2,3\}$ and $\{1,3\}$ a unitary parametric transformation must be applied before a meaningful fidelity is obtained. This unitary transform can be applied either optically or a posteriori. The final state is then $\delta\hat{X}_{\text{para}}^{\pm} = (\sqrt{3})^{\mp 1} \delta\hat{X}_{\text{out}}^{\pm}$, so in the ideal case $\delta\hat{X}_{\text{para}}^{\pm} = \delta\hat{X}_{\text{in}}^{\pm}$. Under ideal conditions and at unitary gain, any one of the access structures can achieve $\mathcal{F} = 1$ corresponding to perfect reconstruction of the secret quantum state, whilst the corresponding adversary structure obtains $\mathcal{F} = 0$.

When no entanglement is used, the maximum fidelity achievable by $\{2,3\}$ and $\{1,3\}$ is $\mathcal{F}_{\{2,3\}}^{\text{clas}} = \mathcal{F}_{\{1,3\}}^{\text{clas}} = 1/2$, whilst $\{1,2\}$ can still achieve $\mathcal{F}_{\{1,2\}}^{\text{clas}} = 1$, so the average fidelity achieved by all permutations of the access structure cannot exceed $\mathcal{F}_{\text{avg}}^{\text{clas}} = 2/3$. This defines the classical boundary for $(2,3)$ threshold quantum state sharing. Note that for general (k,n) threshold quantum state sharing of a coherent state, independent of the dealer protocol, the maximum average fidelity achievable without entanglement resources is $\mathcal{F}_{\text{avg}}^{\text{clas}} = k/n$.

With the $\{1,3\}$ and $\{2,3\}$ protocols being equivalent, our $(2,3)$ threshold quantum state sharing scheme is demonstrated through the implementations of the $\{1,2\}$ and $\{2,3\}$ reconstruction protocols. Figure 2 shows the noise spectra and corresponding inferred Wigner function standard deviation contours for the secret and reconstructed state for the $\{1,2\}$ protocol. The fidelity obtained from these noise spectra is

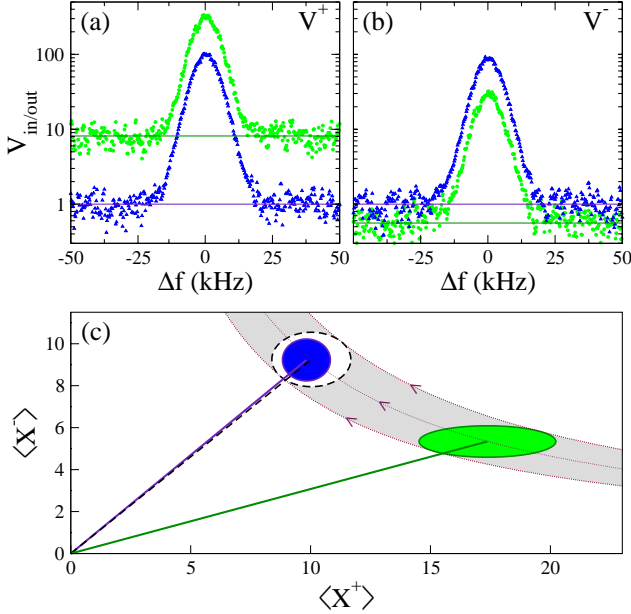


FIG. 3: Experimental results for the $\{2,3\}$ access structure. (a) and (b) show the spectra of the amplitude and phase quadrature variances for the secret (input, blue/dark grey) and reconstructed (output, green/light grey) quantum states. (c) Standard deviation contours of Wigner functions of the secret (blue/dark grey) and reconstructed (green/light grey) quantum states. The dashed circle represents the quantum state $\delta\hat{X}_{\text{para}}^{\pm} = (\sqrt{3})^{\mp 1} \delta\hat{X}_{\text{out}}^{\pm}$ after the a posteriori local unitary parametric operation.

$\mathcal{F}_{\{1,2\}} = 0.93 \pm 0.03$ with $g^+ = 0.94 \pm 0.01$ and $g^- = 0.97 \pm 0.01$. The corresponding adversary structure $\{3\}$ gets a fidelity of $\mathcal{F}_{\{3\}} = 0$ since the share contains no component of the secret state. Figure 2 (d) shows several measured fidelity points as a function of phase space distance, r , between the coherent amplitudes of the secret and reconstructed states. Each fidelity point has a non-zero distance due to mode mismatch, optical losses and imperfect phase locking.

Similarly, Figure 3 shows an example of the secret and reconstructed state for the $\{2,3\}$ protocol. In this case, to allow a direct comparison between the secret and reconstructed states, the inferred Wigner function standard deviation contour of the reconstructed state after the a posteriori local unitary parametric operation is also shown. Figure 4 shows the measured fidelity for a range gains. Around the unitary gain point, we achieve a fidelity of $\mathcal{F}_{\{2,3\}} = 0.63 \pm 0.02$ with $g^+g^- = 1.02 \pm 0.03$. The corresponding adversary structure $\{1\}$ achieves a fidelity of only $\mathcal{F}_{\{1\}} = 0.03 \pm 0.01$. The quantum nature of our protocol is demonstrated by the fidelity averaged over all the access structures $\mathcal{F}_{\text{avg}} = 0.74 \pm 0.04$, which exceeds the classical limit $\mathcal{F}_{\text{avg}}^{\text{clas}} = 2/3$.

Fidelity is a single state dependent measure of the efficacy of quantum information protocols. There are alternative measures which provide complementary information about these processes. One obvious technique is to measure the signal transfer to (\mathcal{T}) , and the additional noise on (\mathcal{V}) , the reconstructed state[12]. Such analysis has been used to characterize quantum non-demolition[13] and quantum teleportation experiments[14]. Unlike the fidelity measure, both \mathcal{T} and \mathcal{V} are invariant to unitary transformations of the reconstructed state. Therefore, for the \mathcal{T} and \mathcal{V} analysis, an a posteriori uni-

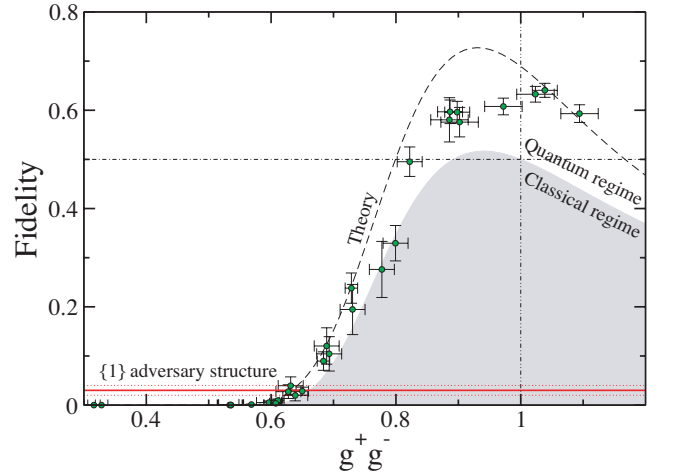


FIG. 4: Experimental fidelity for the $\{2,3\}$ access structure as a function of the product of g^+g^- . Dashed line: calculated theoretical curve with squeezing of -4.5 dB, added noise of $+3.5$ dB, electronic noise of -13 dB with respect to the quantum noise limit, and feed forward detector efficiency of 0.93 . Solid line and dotted lines: experimental fidelity for the adversary structure and error bar. Grey area highlights the classical boundary for the access structure.

tary transform is not required. The signal transfer is given by $\mathcal{T} = T^+ + T^-$, where $T^\pm = \text{SNR}_{\text{out}}^\pm / \text{SNR}_{\text{in}}^\pm$ are the quadrature signal transfer coefficients, with SNR^\pm being the standard signal-to-noise ratios. The additional noise is given by $\mathcal{V} = V_{\text{cv}}^+ V_{\text{cv}}^-$, where $V_{\text{cv}}^\pm = V_{\text{out}}^\pm - |\langle \delta \hat{X}_{\text{in}}^+ \delta \hat{X}_{\text{out}}^+ \rangle|^2 / V_{\text{out}}^\pm$ are the conditional variances. Experimentally, the signal-to-noise ratios that define \mathcal{T} can be obtained from our measured noise spectra (Fig. 2 and 3), whilst V_{cv}^\pm can be determined from the output quadrature variance and the optical quadrature gains $V_{\text{cv}}^\pm = V_{\text{out}}^\pm - (g^\pm)^2$. In the ideal case, any one of the access structures can achieve perfect state reconstruction with $\mathcal{T} = 2$ and $\mathcal{V} = 0$, whilst the corresponding adversary structure obtains no information with $\mathcal{T} = 0$ and $\mathcal{V} = \infty$.

Figure 5 (inset) shows the experimental \mathcal{T} and \mathcal{V} points for the $\{1,2\}$ protocol. We measure a best state reconstruction of $\mathcal{T}_{\{1,2\}} = 1.77 \pm 0.05$ and $\mathcal{V}_{\{1,2\}} = 0.01 \pm 0.01$. Both of these values are close to optimal, being degraded only by optical losses and experimental inefficiencies. Similarly, Figure 5 shows the points for the $\{2,3\}$ protocol for a range of gains, together with the corresponding adversary structure $\{1\}$. The majority of the experimental points are in agreement with the theoretical prediction, with the discrepancies accountable for by drifts in our control system. The accessible region for the $\{2,3\}$ protocol without entanglement is illustrated by the shaded region. The quantum nature of the state reconstruction is demonstrated by the experimental points which exceed this classical region. For the $\{2,3\}$ protocol we measure a lowest reconstruction noise of $\mathcal{V}_{\{2,3\}} = 0.46 \pm 0.08$ and a largest signal transfer of $\mathcal{T}_{\{2,3\}} = 1.03 \pm 0.05$. Points with $\mathcal{T} > 1$ ex-

ceed the information cloning limit[14] and demonstrate that the $\{2,3\}$ protocol has better access to information encoded on the secret state than any other parties. The adversary structure obtains a mean $\mathcal{T}_{\{1\}} = 0.41 \pm 0.01$ and $\mathcal{V}_{\{1\}} = 3.70 \pm 0.08$. The separation of the adversary structure \mathcal{T} and \mathcal{V} points from that of the $\{2,3\}$ protocol in Figure 5 illustrates that in such a protocol the access structure performs far better than any adversary structure.

Our experimental demonstration of $(2,3)$ threshold quantum state sharing is the first application of continuous variable tripartite entanglement. Furthermore, it is extendable to an arbitrary (k,n) scheme, without a corresponding scale-up of the required quantum resources[15]. The implementation of quantum state sharing broadens the scope of quantum information networks allowing quantum communication between multiple nodes, whilst providing security against malicious parties in the network as well as node and channel failures.

We wish to thank Timothy Ralph, Tomáš Tyc, Roman Schnabel and Hans Bachor for useful discussions and the support of the Australian Research Council and iCORE.

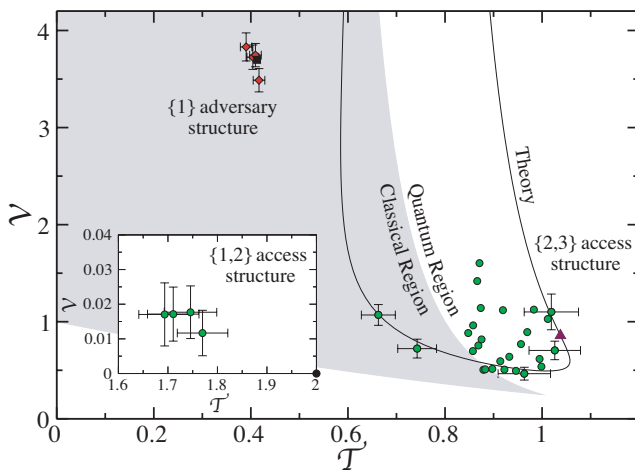


FIG. 5: Experimental signal transfer (\mathcal{T}) and additional noise (\mathcal{V}) for the $\{2,3\}$ access structure (green/light grey circles), and the adversary structure (red/dark grey diamonds). Solid line: calculated theoretical curve for varying gain with same parameters as in Figure 4. Triangle symbol: unitary gain point for the $\{2,3\}$ access structure. Square symbol: calculated theoretical point for the adversary structure. Grey area: the classical region for the $\{2,3\}$ access structure. (inset) Experimental \mathcal{T} and \mathcal{V} for the $\{1,2\}$ access structure (green/light grey circles) and the theoretical point (black circles).

-
- [1] A. Shamir, *Comm. of the ACM* **22**, 612 (1979).
 - [2] M. Hillery, V. Bužek and A. Berthiaume, *Phys. Rev. A* **59**, 1829 (1999); A. Karlsson, M. Koashi and N. Imoto, *Phys. Rev. A* **59**, 162 (1999); W. Tittel, H. Zbinden and N. Gisin, *Phys. Rev. A* **63**, 042301 (2001).
 - [3] J. I. Cirac, P. Zoller, H. J. Kimble and H. Mabuchi, *Phys. Rev. Lett.* **78**, 3221 (1997).
 - [4] R. Cleve, D. Gottesman and H-K. Lo, *Phys. Rev. Lett.* **83**, 648 (1999).
 - [5] T. Tyc and B. C. Sanders, *Phys. Rev. A* **65**, 42310 (2002).
 - [6] Z. Y. Ou, S. F. Pereira, H. J. Kimble and K. C. Peng, *Phys. Rev. Lett.* **68**, 3663 (1992).
 - [7] W. P. Bowen, R. Schnabel, P. K. Lam and T. C. Ralph, *Phys. Rev. Lett.* **90**, 043601 (2003).
 - [8] A. M. Lance, T. Symul, W. P. Bowen, T. Tyc, B. C. Sanders and P. K. Lam, *New J. of Phys.* **5**, 4.1 (2003).
 - [9] A. Furusawa, *et al.*, *Nature* **282**, 706 (1998).
 - [10] L-M. Duan, G. Giedke, J. I. Cirac and P. Zoller, *Phys. Rev. Lett.* **84**, 2722 (2000).
 - [11] B. Schumacher, *Phys. Rev. A* **51**, 2738 (1995).
 - [12] T. C. Ralph and P. K. Lam, *Phys. Rev. Lett.* **81**, 5668 (1998).
 - [13] J. -Ph. Poizat, J. -F. Roch, and P. Grangier, *Ann. Phys. (Paris)* **19**, 265 (1994).
 - [14] W. P. Bowen, *et al.*, *Phys. Rev. A* **67**, 032302 (2003).
 - [15] T. Tyc, D. J. Rowe and B. C. Sanders, *J. Phys. A:Math. Gen.* **36**, 7625 (2003).
 - [16] This aspect of de-coherence will be described in detail in a later publication.